American Journal of Engineering Research (AJER)
e-ISSN: 2320-0847 p-ISSN : 2320-0936
Volume-5, Issue-4, pp-01-14
www.ajer.org
Research Paper Open Access

Axisymmetric Problem in Thermoporoelastic Medium

Rajneesh Kumar[1], Satinder Kumar[2] and M. G. Gourla[3]
[1]*Department of Mathematics, Kurukshetra University, Kurukshetra, Haryana, India*
[2]*Department of Mathematics, Govt. Degree College Chowari (Chamba), Himachal Pradesh, India*
[3]*Department of Mathematics, Himachal Pradesh University, Shimla-171005, India*

ABSTRACT: *The present investigation deals with the response of thermomechanical sources in a thermoporoelastic medium. Laplace and Hankel transforms are applied to investigate the problem. As an application of the approach concentrated source and source over circular region in the time domain and frequency domain are taken to illustrate the utility of the approach. The expressions for displacement components, stress components, pore pressure and temperature change are obtained in the transformed domain. To obtain the resulting quantities in the physical domain,a numerical inversion techniques are applied. Effect of porosity is shown on the resulting quantities. A particular case of interest is also deduced from the present investigation.*

Keywords*: thermoporoelastic medium, Laplace transform, Hankel transform, concentrated source , source over circular region.*

I. INTRODUCTION

The effect of temperature on the behaviour of medium is a crucial problem and is important for several branches of engineering. Some of the important cases are the disposal of high-level radioactive waste, the extraction of oil or geothermal energy, the storage of hot fluid, and the road subgrade or the furnace foundation, which are usually subjected to cyclic changes of temperature. In addition, the case of underground nuclear explosion, the case of sudden heat radiation due to accidents involving nuclear waste buried in the ground are the other applications of the thermodynamics in engineering.

For the thermoporoelastisity problems, coupled thermal and poro-mechanical processes play an important role in a number of problems of interest in the geomechanics such as stability of boreholes and permeability enhancement in geothermal reservoirs. A thermoporoelastic approach combines the theory of heat conduction with poroelastic constitutive equations and coupling the temperature fields with the stresses and pore pressure.
Biot [1] proposed a general theory of three dimensional deformations of liquid saturated porous solid. Liu et al. [2] discussed the thermo-elastodynamic response of a spherical cavity in saturated poroelastic medium.They also discussed mode of a spherical cavity's thermo-elastodynamic response in a saturated porous medium for non-torsional load [3]. Abousleiman and Ekbote [4] obtained the solutions for the inclined borehole in a porothermoelastic transversely isotropic medium.

Kumar and Hundal [5] discussed the symmetric wave propagation in a fluid saturated incompressible porous medium. Kumar and Rupender [6] discussed the elastodynamics of axi-symmetric deformation in magneto-micropolar generalized thermoelastic medium. Bai and Li [7] obtained the solution for cylindrical cavety in a saturated thermoporoelastic medium. Bai [8] also discussed the thermal response of saturated porous spherical body containing a cavity under several boundary conditions. Jabbari and Dehbani [9] obtained an exact solution for classic coupled thermoelasticity in axisymmetric cylinder.They also obtained an exact solution for quasi-static poro- thermoelastic problem in spherical coordinate [10]. Jabbari et.al. [11] also discuss thermal buckling analysis of functionally graded thin circular plate made of saturated porous materials.

Belotserkovets and Prevost [12] discussed the thermoporoelastic response of a fluid saturated porous sphere. Hou,et. al. [13] discussed the three dimensional green's function for transversely isotropic thermoporoelastic biomaterial. Gelet et. al. [14]discussed the borehole stability analysis in a thermoporoelastic duel-porosity medium. Li et al. [15] obtained the general steady state solution for transversely isotropic thermoporoelastic

medium in three dimension . Mukhopadhyay and Kumar [16] discuss the analysis of phase-lag effects on wave propagation in a thick plate under axisymmetric temperature distribution.

Mixed variation principal for dynamic response of thermoelastic and poroelastic continua was discussed by Apostolakis and Dargus [17]. Hou, et. al. [18] discussed the three dimensional Green's function for transversely isotropic thermoporoelastic biomaterial. He et al.[19] studied the dynamic simulation of landslide based on thermoporoelastic approach. Nguyen et al.[20] discussed the analytical study of freezing behaviour of a cavity in thermoporoelastic medium. Wu et al. [21] presented a refined theory of axisymmetric thermoporoelastic circular cylinder.

In the present paper, we obtain the components of displacement, stress, pore pressure and temperature change due to concentrated source and source over circular region in the time domain and frequency domain in thermoporoelastic medium with incompressible fluid. Laplace and Hankel transforms are used to investigate the problem. Numerical inversion techniques are applied to obtain the resulting quantities in a physical domain. The resulting quantities are shown graphically to depict the effect of porosity.

II. GOVERNING EQUATIONS

Following Jabbari and Dehbani [22], the field equations are

$$(\lambda+\mu)\nabla\nabla.\vec{u}+\mu\nabla^2\vec{u}-\alpha\nabla p-\beta\nabla T=\rho\frac{\partial^2\vec{u}}{\partial t^2} \quad , \qquad (1)$$

$$\frac{k}{\gamma_w}\nabla^2 p-\alpha_p\dot{p}-Y\dot{T}-\alpha div\dot{\vec{u}}=0 \quad , \qquad (2)$$

$$K\nabla^2 T-ZT_0\dot{T}+YT_0\dot{p}-\beta T_0 div\dot{\vec{u}}=0 \quad , \qquad (3)$$

$$\sigma_{ij}=\lambda u_{k,k}\delta_{ij}+\mu\left(u_{i,j}+u_{j,i}\right)-\alpha p\delta_{ij}-\beta T\delta_{ij} \quad , \qquad (4)$$

where $\vec{u}$ is the displacement component, p is the pore pressure, ρ is the bulk mass density , $\alpha=1-\frac{C_s}{C}$ is the Biot's coefficient , $C_s=3(1-2v_s)/E_s$ is the coefficient of volumetric compression of solid grain , with E_s and v_s being the elastic modulus and Poisson's ratio of solid grain , $C=3(1-2v)/E$ is the coefficient of volumetric compression of solid skeleton , with E and v being the elastic modulus and Poisson's ratio of solid skeleton , T_0 is initial reference temperature , $\beta=\frac{3\alpha_s}{C}$ is the thermal expansion factor , α_s is the coefficient of linear thermal expansion of solid grain ,$Y=3(n\alpha_w+(\alpha-n)\alpha_s)$ and $\alpha_p=n(C_w-C_s)+\alpha C_s$ are coupling parameters , α_w and C_w are the coefficients of linear thermal expansion and volumetric compression of pure water , n is the porosity , k is the hydraulic conductivity , γ_w is the unit of pore water and $Z=\frac{(1-n)\rho_s C_s+n\rho_w C_w}{T_0}$ is coupling parameter , ρ_w and ρ_s are densities of pore water and solid grain and C_w and C_s are heat capacities of pore water and solid grain and K is the coefficient of heat conductivity.

III. FORMULATION AND SOLUTION OF THE PROBLEM

We consider a homogeneous, incompressible fluid saturated thermal conducting poroelastic medium at uniform temperature T_0 in the undeformed state. We take cylindrical polar coordinate system (r,θ,z) and consider a two dimensional axi-symmetric problem with symmetry about z-axis, so that all the quantities are remain independent of θ and $\frac{\partial}{\partial\theta}=0$. The complete geometry of the problem is shown in the figure 1(a),1(b). Since we are considering two dimensional problem, so we assume the components of displacement vector $\vec{u}$ of the fom

$$\vec{u}=(u_r,0,u_z) \quad . \qquad (5)$$

Equations (1)-(3) with the aid of (5) can be written as:

$$\mu\left[\left(\nabla^2u_r-\frac{1}{r^2}u_r\right)e_r+\nabla^2u_z e_z\right]+(\lambda+\mu)\left[\left(\frac{\partial^2u_r}{\partial r^2}+\frac{1}{r}\frac{\partial u_r}{\partial r}+\frac{\partial^2u_z}{\partial r\partial z}\right)e_r+\left(\frac{\partial^2u_r}{\partial z\partial r}+\frac{1}{r}\frac{\partial u_r}{\partial z}+\frac{\partial^2u_z}{\partial z^2}\right)e_z\right]-$$
$$\alpha\left[\frac{\partial p}{\partial r}e_r+\frac{\partial p}{\partial z}e_z\right]-\beta\left[\frac{\partial T}{\partial r}e_r+\frac{\partial T}{\partial z}e_z\right]-\rho\left[\frac{\partial^2u_r}{\partial t^2}e_r+\frac{\partial^2u_z}{\partial t^2}e_z\right]=0 \qquad (6)$$

$$\frac{k}{\gamma_w}\left[\frac{\partial^2p}{\partial r^2}+\frac{1}{r}\frac{\partial p}{\partial r}+\frac{\partial^2p}{\partial z^2}\right]-\alpha_p\frac{\partial p}{\partial t}-Y\frac{\partial T}{\partial t}-\alpha\left[\frac{\partial^2u_r}{\partial t\partial r}+\frac{1}{r}\frac{\partial u_r}{\partial t}+\frac{\partial^2u_z}{\partial z\partial t}\right]=0 \qquad (7)$$

$$K\left[\frac{\partial^2T}{\partial r^2}+\frac{1}{r}\frac{\partial T}{\partial r}+\frac{\partial^2T}{\partial z^2}\right]-ZT_0\frac{\partial T}{\partial t}-YT_0\frac{\partial p}{\partial t}-\beta T_0\left[\frac{\partial^2u_r}{\partial t\partial r}+\frac{1}{r}\frac{\partial u_r}{\partial t}+\frac{\partial^2u_z}{\partial z\partial t}\right]=0 \qquad (8)$$

We define the non-dimensional quantities

$$r'=\frac{\omega^*}{c_1}r,\ z'=\frac{\omega^*}{c_1}z\ ,\ u_r'=\frac{\omega^*}{c_1}u_r\ ,u_z'=\frac{\omega^*}{c_1}u_z\ ,p'=\frac{p}{\beta T_0}\ ,c_1^2=\frac{\lambda+2\mu}{\rho}\ ,\quad t'=\omega^*t,\quad T'=\frac{T}{T_0}\ ,\ \sigma_{zz}'=\frac{\sigma_{zz}}{\beta T_0},\sigma_{zr}'=\frac{\sigma_{zr}}{\beta T_0} \qquad (9)$$

where ω^* is the constant having the dimensions of frequency.

Using dimensionless quantities defined by (9), in the equations (6)-(8) yield

$\frac{\partial e}{\partial r} + a_1(\nabla^2 - \frac{1}{r^2})u_r - a_2\frac{\partial p}{\partial r} - a_3\frac{\partial T}{\partial r} = a_4\frac{\partial^2 u_r}{\partial t^2}$, (10)

$\frac{\partial e}{\partial z} + a_1\nabla^2 u_z - a_2\frac{\partial p}{\partial z} - a_3\frac{\partial T}{\partial z} = a_4\frac{\partial^2 u_z}{\partial t^2}$, (11)

$b_1\nabla^2 p - b_2\frac{\partial p}{\partial t} - b_3\frac{\partial T}{\partial t} - \frac{\partial e}{\partial t} = 0$, (12)

$b_4\nabla^2 T - b_5\frac{\partial T}{\partial t} + b_6\frac{\partial p}{\partial t} - \frac{\partial e}{\partial t} = 0$, (13)

where

$a_1 = \frac{\mu}{\lambda+\mu}$, $a_2 = \frac{\alpha\beta T_0}{\lambda+\mu}$, $a_3 = \frac{\beta T_0}{\lambda+\mu}$, $a_4 = \frac{\rho c_1^2}{\lambda+\mu}$, $b_1 = \frac{k\omega^*\beta T_0}{\gamma_w \alpha c_1^2}$, $b_2 = \frac{\alpha_p \beta T_0}{\alpha}$

$b_3 = \frac{YT_0}{\alpha}$, $b_4 = \frac{K\omega^*}{\beta c_1^2}$, $b_5 = \frac{ZT_0}{\beta}$, $b_6 = YT_0$,

and $e = \frac{\partial u_r}{\partial r} + \frac{1}{r}u_r + \frac{\partial u_z}{\partial z}$, $\nabla^2 = \frac{\partial^2}{\partial r^2} + \frac{1}{r}\frac{\partial}{\partial r} + \frac{\partial^2}{\partial z^2}$ (14) To simplify the problem, we introduce the potential functions as:

$u_r = \frac{\partial \Phi}{\partial r} - \frac{\partial \Psi}{\partial z}$, $u_z = \frac{\partial \Phi}{\partial z} + \frac{\partial \Psi}{\partial r} + \frac{\Psi}{r}$ (15)

Using (14) and (15) eqs. (10)-(13) become

$(1 + a_1)\nabla^2\Phi - a_2 p - a_3 T - a_4\frac{\partial^2 \Phi}{\partial t^2} = 0$, (16)

$a_1\nabla^2\Psi - \frac{a_1}{r^2}\Psi - a_4\frac{\partial^2 \Psi}{\partial t^2} = 0$, (17)

$b_1\nabla^2 p - b_2\frac{\partial p}{\partial t} - b_3\frac{\partial T}{\partial t} - \frac{\partial}{\partial t}[\nabla^2\Phi] = 0$, (18)

$b_4\nabla^2 T - b_5\frac{\partial T}{\partial t} + b_6\frac{\partial p}{\partial t} - \frac{\partial}{\partial t}[\nabla^2\Phi] = 0$. (19)

We define the Laplace and Hankel transforms as follows:

$\bar{f}(s) = \int_0^\infty f(t)e^{-st}\,dt$, (20)

$\tilde{f}(\xi, z, s) = \int_0^\infty \bar{f}(r, z, s) r J_n(r\xi) dr$, (21)

where $J_n(X)$ is the Bessel function of the first kind of index n.

Applying integral transforms defined by (20) and (21) on (16)-(19), we obtain

$-\xi^2\tilde{\bar{\Phi}} + \frac{d^2\tilde{\bar{\Phi}}}{dz^2} - A_1\tilde{\bar{p}} - A_2\tilde{\bar{T}} - A_3\tilde{\bar{\Phi}} = 0$, (22)

$-\xi^2\tilde{\bar{\Psi}} + \frac{d^2\tilde{\bar{\Psi}}}{dz^2} - A_4\tilde{\bar{\Psi}} = 0$, (23)

$-\xi^2\tilde{\bar{p}} + \frac{d^2\tilde{\bar{p}}}{dz^2} - B_3\xi^2\tilde{\bar{\Phi}} - B_3\frac{d^2\tilde{\bar{\Phi}}}{dz^2} - B_1\tilde{\bar{p}} - B_2\tilde{\bar{T}} = 0$, (24)

$-\xi^2\tilde{\bar{T}} + \frac{d^2\tilde{\bar{T}}}{dz^2} - B_6\xi^2\tilde{\bar{\Phi}} - B_6\frac{d^2\tilde{\bar{\Phi}}}{dz^2} - B_4\tilde{\bar{T}} - B_5\tilde{\bar{p}} = 0$ (25)

where $A_1 = \frac{a_2}{1+a_1}$, $A_2 = \frac{a_3}{1+a_1}$, $A_3 = \frac{a_4 s^2}{1+a_1}$, $A_4 = \frac{a_4 s^2}{a_1}$, $B_1 = \frac{b_2 s}{b_1}$, $B_2 = \frac{b_3 s}{b_1}$ $B_3 = \frac{s}{b_1}$, $B_4 = \frac{b_5 s}{b_4}$, $B_5 = \frac{b_6 s}{b_4}$, $B_6 = \frac{b_7 s}{b_4}$.

Eliminating $\tilde{\bar{p}}$ and $\tilde{\bar{T}}$ from above equations, we obtain

$\left[\frac{d^6}{dz^6} + D_1\frac{d^4}{dz^4} + D_2\frac{d^2}{dz^2} + D_3\right]\tilde{\bar{\Phi}} = 0$, (26)

$\left(\frac{d^2}{dz^2} - \xi^2\right)\tilde{\bar{\Psi}} - A_4\tilde{\bar{\Psi}} = 0$, (27)

where

$D_1 = -3\xi^2 - (B_1 + B_4) - A_3 - A_1B_3 - A_2B_6$, $D_2 = -3\xi^4 - 2(B_1 + B_4)\xi^2 + (B_1B_4 - B_2B_5) + 2A_3\xi^2 + (B_1 + B_4)A_3 + 2A_1A_3\xi^2 - A_1(B_2B_6 - B_3B_4) + 2A_2B_6\xi^2 - A_2(B_3B_5 - B_1B_6)$,

$D_3 = \xi^6 - (B_1 + B_4)\xi^4 - \xi^2(B_1B_4 - B_2B_5) - (B_1 + B_4)A_3\xi^2 - A_3\xi^4 - A_3(B_1B_4 - B_2B_5) - A_1A_3\xi^2 + A_1\xi^2(B_2B_6 - B_3B_4) - A_2B_6\xi^4 + A_2\xi^2(B_3B_5 - B_1B_6)$.

Solving (26) and (27) and assuming that $\tilde{\bar{\Phi}}, \tilde{\bar{\Psi}}, \tilde{\bar{p}}$ and $\tilde{\bar{T}} \to 0$ as $z \to \infty$ we obtain the value of $\tilde{\bar{\Phi}}, \tilde{\bar{\Psi}}, \tilde{\bar{p}}$ and $\tilde{\bar{T}}$ as

$\tilde{\bar{\Phi}} = E_1e^{-m_1z} + E_2e^{-m_2z} + E_3e^{-m_3z}$, (28)

$\tilde{\bar{\Psi}} = E_4e^{-m_4z}$, (29)

$\tilde{\bar{p}} = r_1E_1e^{-m_1z} + r_2E_2e^{-m_2z} + r_3E_3e^{-m_3z}$, (30)

$\tilde{\bar{T}} = s_1E_1e^{-m_1z} + s_2E_2e^{-m_2z} + s_3E_3e^{-m_3z}$ (31)

where m_1, m_2, m_3 are the roots of the equation (26) found with the help of cardon method and $m_4 = \sqrt{A_5}$

where $A_5 = \xi^2 + a_4$

and the coupling constants are given by

$$r_i = \frac{B_3(m_i^2-\xi^2)^2+(B_2B_6-B_3B_4)(m_i^2-\xi^2)}{(m_i^2-\xi^2)^2-(B_1+B_4)(m_i^2-\xi^2)+(B_1B_4-B_2B_5)} \quad (32)$$

$$s_i = \frac{B_6(m_i^2-\xi^2)^2+(B_3B_5-B_1B_6)(m_i^2-\xi^2)}{(m_i^2-\xi^2)^2-(B_1+B_4)(m_i^2-\xi^2)+(B_1B_4-B_2B_5)} \quad (33)$$

(i=1,2,3) .

The displacement components $\widetilde{\overline{u_r}}$ and $\widetilde{\overline{u_z}}$ are obtained with the aid of (20)-(21) and (28)-(29) as

$\widetilde{\overline{u_r}} = -E_1\xi e^{-m_1 z} - E_2\xi e^{-m_2 z} - E_3\xi e^{-m_3 z} + E_4 m_4 e^{-m_4 z}$, (34)

$\widetilde{\overline{u_z}} = -E_1 m_1 e^{-m_1 z} - E_2 m_2 e^{-m_2 z} - E_3 m_3 e^{-m_3 z} + E_4\xi e^{-m_4 z}$ (35)

BOUNDARY CONDITIONS

The boundary conditions at z = 0 are

$\sigma_{zz} = -F_1F(r,t), \sigma_{zr} = -F_2F(r,t), p = F_3F(r,t), \frac{\partial T}{\partial x_3} = F_4F(r,t)$ (36)

where F_1, F_2 are the magnitudes of the forces , F_3 is the constant pressure applied on the boundary and $F_4$is the constant temperature applied on the boundary. $F(r,t)$ is a known function of r and t.

Applying Laplace and Hankel transforms defined by (20)and (21) on (36) and with the aid of (9) , we obtain

$\widetilde{\overline{\sigma_{zz}}} = -F_1\tilde{\bar{F}}(\xi,s), \widetilde{\overline{\sigma_{zr}}} = -F_2\tilde{\bar{F}}(\xi,s), \tilde{\bar{p}} = F_3\tilde{\bar{F}}(\xi,s), \frac{\partial\tilde{\bar{T}}}{\partial x_3} = F_4\tilde{\bar{F}}(\xi,s)$,at z = 0(37)

where

$\widetilde{\overline{\sigma_{zz}}} = R_1\xi\widetilde{\overline{u_r}} + R_2\frac{d\widetilde{\overline{u_z}}}{dz} - \alpha\tilde{\bar{p}} - \tilde{\bar{T}}$, (38)

$\widetilde{\overline{\sigma_{zr}}} = R_3\left[\frac{d\widetilde{\overline{u_r}}}{dz} - \xi\widetilde{\overline{u_z}}\right]$ (39)

and $R_1 = \frac{\lambda}{\beta T_0}$, $R_2 = \frac{\lambda+2\mu}{\beta T_0}$, $R_3 = \frac{\mu}{\beta T_0}$

Case 1: for normal force $F_2 = F_3 = F_4 = 0$

Case 2: for shear force $F_1 = F_3 = F_4 = 0$

Case 3: For pressure source $F_1 = F_2 = F_4 = 0$

Case 4: For thermal source $F_1 = F_2 = F_3 = 0$

Substituting the values of $\widetilde{\overline{u_r}}, \widetilde{\overline{u_z}}, \tilde{\bar{p}}$ and $\tilde{\bar{T}}$from(34),(35) and (30),(31) in the boundary condition (37) and with help of (38) and (39), after some simplifications, we obtain

$\widetilde{\overline{\sigma_{zz}}} = \frac{1}{\Delta}[d_1\Delta_1 e^{-m_1 z} + d_2\Delta_2 e^{-m_2 z} + d_3\Delta_3 e^{-m_3 z} + d_4\Delta_4 e^{-m_4 z}]$, (40)

$\widetilde{\overline{\sigma_{zr}}} = \frac{1}{\Delta}[d_5\Delta_1 e^{-m_1 z} + d_6\Delta_2 e^{-m_2 z} + d_7\Delta_3 e^{-m_3 z} + d_8\Delta_4 e^{-m_4 z}]$, (41)

$\tilde{\bar{p}} = \frac{1}{\Delta}[r_1\Delta_1 e^{-m_1 z} + r_2\Delta_2 e^{-m_2 z} + r_3\Delta_3 e^{-m_3 z}]$, (42)

$\tilde{\bar{T}} = \frac{1}{\Delta}[s_1\Delta_1 e^{-m_1 z} + s_2\Delta_2 e^{-m_2 z} + s_3\Delta_3 e^{-m_3 z}]$, (43)

where

$\Delta = d_1d_8(-m_3r_2s_3 + m_2r_3s_2) - d_2d_8(-m_3r_1s_3 + m_1r_3s_1) + d_3d_8(-m_2r_1s_2 + m_1r_2s_1) - d_4d_5(-m_3r_2s_3 + m_2r_3s_2 - d_4d_6 - m_3r_1s_3 + m_1r_3s_1 - d_4d_7 - m_2r_1s_2 + m_1r_2s_1$,

$d_i = -R_1\xi^2 + R_2m_i^2 - \alpha r_i - s_i$ where (i=1,2,3) , $d_4 = \xi m_4(R_1 - R_2)$

$d_j = 2\xi m_j R_3$ where (j=5,6,7) , $d_8 = -R_3(m_4^2 + \xi^2)$,

and $\Delta_1, \Delta_2, \Delta_3, \Delta_4$ are obtained by replacing$[-F_1, -F_2, F_3, F_4]^T$ in Δ.

APPLICATIONS:

TIME DOMAIN:

CASE 1.CONCENTRATED SOURCE:

The solutions due to concentrated source is obtained by substituting

$F(r,t) = F_1(r)\eta(t)$, (44)

where

$F_1(r) = \frac{1}{2\pi r}\delta(r)$. (45)

Applying Laplace and Hankel transform on (44) and (45), we obtain

$\tilde{\bar{F}}(\xi,s) = \frac{1}{2\pi}\bar{\eta}(s)$

CASE 2:SOURCE OVER CIRCULAR REGION:

The solution due to source over the circular region of non-dimensional radius a is obtained by setting $F(r,t) = F_1(r)\eta(t)$,

where

$F_1(r) = \frac{1}{\pi a^2} H(a - r)$.
Applying Laplace and Hankel transforms on these quantities, we obtain,
$\tilde{\bar{F}}(\xi, s) = \frac{1}{\pi a \xi} J_1(a\xi)\bar{\eta}(s)$
In both the cases, we have taken $\eta(t) = H(t)$, so Laplace transform of $\eta(t)$ gives, $\bar{\eta}(s) = 1/s$.

FREQUENCY DOMAIN:
In this case we assume the time harmonic behaviour as
$(u_r, u_z, p, T)(r, z, t) = (u_r, u_z, p, T)(r, z, t)e^{i\omega t}$,
In frequency domain, we take $\eta(t) = e^{i\omega t}$.
The expressions for displacement, stress and pore pressure and thermal source in frequency domain can be obtained by replacing s by $i\omega$ in the expressions of time domain (40) - (43) along with $\bar{\eta}(s)$ to be replaced by $e^{i\omega t}$ for concentrated source.

SPECIAL CASE
In the absence of porosity effect, we obtain the stress components and temperature change as

$$\tilde{\bar{\sigma}}_{zz} = \frac{1}{\Delta_{10}}[d_9\Delta_5 e^{-m_5 z} + d_{10}\Delta_6 e^{-m_6 z} + d_4\Delta_4 e^{-m_4 z}], \quad (46)$$

$$\tilde{\bar{\sigma}}_{zr} = \frac{1}{\Delta_{10}}[d_{11}\Delta_5 e^{-m_5 z} + d_{12}\Delta_6 e^{-m_6 z} + d_8\Delta_4 e^{-m_4 z}], \quad (47)$$

$$\tilde{\bar{T}} = \frac{1}{\Delta_{10}}[s_5\Delta_5 e^{-m_5 z} + s_6\Delta_6 e^{-m_6 z}] \quad (48)$$

where
$\Delta_{10} = s_6 m_6 d_8 d_9 + s_5 m_5 d_8 d_{10} - s_6 m_6 d_{11} d_4 + s_5 m_5 d_{12} d_4$,
$d_9 = -R_1\xi^2 + R_2 m_5^2 - s_5$, $d_{10} = -R_1\xi^2 + R_2 m_6^2 - s_6$, $d_4 = \xi m_4(R_1 - R_2)$
$d_{11} = 2\xi m_5 R_3$, $d_{12} = 2\xi m_6 R_3$, $d_8 = -R_3(m_4^2 + \xi^2)$,
and $\Delta_5, \Delta_6, \Delta_7$ are obtained by replacing $[-F_1, -F_2, F_4]^T$ in Δ_{10}.
Taking $F_2 = F_4 = 0$, $F_1 = F_4 = 0, F_1 = F_2 = 0$ in equations (46)-(48) respectively, we obtain the stress components and temperature change for normal force, tangential forces and thermal source respectively.

INVERSION OF THE TRANSFORM
The transformed displacements, stresses, pore pressure and temperature are functions of the parameters of the Laplace and Hankel transforms s and ξ respectively and hence are of the form $\tilde{\bar{f}}(\xi, z, s)$.To obtain the solution of the problem in the physical domain, we invert the Laplace and Hankel transforms by using the method described by Kumar and Deswal [23].

IV. NUMERICAL RESULTS AND DISCUSSION

With the view of illustrating the theoretical results and for numerical discussion we take a model for which the value of the various physical parameters are taken from Jabbari and Dehbani [22]:
$E = 6 \times 10^5$, $\nu = 0.3$, $T_0 = 293$, $K_s = 2 \times 10^{10}$, $K_w = 5 \times 10^9$, $K = 0.5$,
$\alpha_s = 1.5 \times 10^{-5}$, $\alpha_W = 2 \times 10^{-4}$, $c_s = 0.8$, $c_w = 4.2$, $\rho_s = 2.6 \times 10^6$, $\rho_w = 1 \times 10^6$, $\alpha = 1$, $F_1 = F_2 = F_3 = F_4 = 1$.
The values of components of stress σ_{zz}, σ_{zr}, pore pressure p and temperature change T for incompressible fluid saturated thermoporoelastic medium (FSTM) and empty porous thermoelastic medium (EPM) are shown due concentrated source and source applied over the circular region. The computation are carried out for two values of dimensionless time t=0.1 and t=0.5 at z=1 in the range $0 \le r \le 10$.

The solid lines either without central symbols or with central symbols represents the variations for t=0.1, whereas the dashed lines with or without central symbols represents the variations for t=0.5.Curves without central symbols correspond to the case of FSTM whereas those with central symbols corresponds to the case of EPM.

TIME DOMAIN NORMAL FORCE
Fig. 2 shows the variation of normal stress component σ_{zz} w.r.t distance r due to concentrated force. The value of σ_{zz} starts with initial increase and then oscillates for FSTM as r increases for both values of time. In case of EPM, the value of σ_{zz} increases for the range $0 \le r \le 1.5$ and then oscillates oppositely as r increases for both values of time.

Behaviour of shear stress component σ_{zr} w.r.t distance r due to concentrated force is shown in figure 3. The value of σ_{zr} increases for the range $0 \leq r \leq 2.5$ and then oscillates for FSTM as r increases whereas in case of EPM, its value oscillates oppositely as r increases for both values of time.

Fig. 4 shows the variation of pore pressure p w.r.t distance r due to concentrated source. The value of p decreases for the range $0 \leq r \leq 2.5$ and then start oscillating for FSTM as r increases for both values of time.
Fig. 5 depicts the variation of temperature T w.r.t distance r due to concentrated source. The value of T decreases for the range $0 \leq r \leq 2.4$ and then start oscillating for time t=0.1 whereas for the time t=0.5 its value converges near the boundary surface for FSTM as r increases. In case of EPM, the value of T oscillates oppositely as r increases for both values of time.

Fig. 6 shows the variation of normal stress σ_{zz} w.r.t distance r due to force over circular region. The value of σ_{zz} start with initial increase and then oscillates for FSTM and EPM as r increases for both value time.
Fig. 7 shows the variation of shear stress component σ_{zr} w.r.t distance r due to force over circular region. The value of σ_{zr} first increases and then starts oscillates for FSTM and the value of σ_{zr} for EPM oscillating oppositely as r increases for both value time .

Behaviour of pore pressure p w.r.t distance r due to force over circular region is shown in figure 8. The value of p decreases for the range $0 \leq r \leq 2.4$ and then starts oscillates for FSTM as r increases for time t=0.1 whereas for the time t=0.5 its value first decreases and then converges near the boundary surface as r increases.
Behaviour of temperature T w.r.t distance r due to force over circular region is shown in figure 9. The value of T for the time t=0.1 first decreases and then starts oscillates whereas for the time t=0.5 its value with initial increase converges near the boundary surface for FSTM. The value of T for EPM oscillates oppositely as r increases for both values time.

PRESSURE SOURCE

Fig. 10 shows the variation of normal stress component σ_{zz} w.r.t distance r due to concentrated force. The value of σ_{zz} decrease sharply for the range $0 \leq r \leq 2.2$ and then oscillates for FSTM as r increases for time t=0.1 whereas for the time t=0.5 the value of σ_{zz} shows initial decrease and then converges near the boundary surface.
Behaviour of shear stress component σ_{zr} w.r.t distance r due to concentrated force is shown in figure 11. The value of σ_{zr} decrease sharply for the range $0 \leq r \leq 2.3$ and then oscillates for FSTM as r increases for time t=0.1 whereas for the time t=0.5 the value of σ_{zr} first increases and then oscillates as r increases.
Fig. 12 depicts the variation of pore pressure p w.r.t distance r due to concentrated force. The value of p increases sharply for the range $0 \leq r \leq 2.4$ and then oscillates for FSTM as r increases for both values of time.
Fig. 13 shows the variation of temperature T w.r.t distance r due to concentrated force. The value of T increase sharply for the range $0 \leq r \leq 2.7$ and then oscillates for FSTM as r increases for time t=0.1 whereas for the time t=0.5 the value of T start with initial increase and then oscillates as r increases.
Fig. 14 shows the variation of normal stress component σ_{zz} w.r.t distance r due to force over circular region. The value of σ_{zz} decrease sharply for the range $0 \leq r \leq 2.2$ and then oscillates for FSTM as r increases for time t=0.1 whereas for the time t=0.5 the value of σ_{zz} shows initial decrease and then converges near the boundary surface.

Fig. 15 shows the variation of shear stress component σ_{zr} w.r.t distance r due to force over circular region. The value of σ_{zr} first decreases and then oscillates for FSTM as r increases for time t=0.1 whereas for the time t=0.5 the value of σ_{zr} increases for the range $0 \leq r \leq 4.5$ and then oscillates as r increases.
Fig. 16 depicts the variation of pore pressure p w.r.t distance r due to force over circular region. With initial increase, the value of p oscillates for FSTM as r increases for time t=0.1 whereas for the time t=0.5 the value of p increases sharply for the range $0 \leq r \leq 2.5$ and then oscillates as r increases.
Fig. 17 depicts the variation of temperature T w.r.t distance r due to force over circular region. The value of T increases for the range $0 \leq r \leq 2.4$ and then oscillates for FSTM as r increases for both values of time.

THERMAL SOURCE

Fig. 18 shows the variation of normal stress component σ_{zz} w.r.t distance r due to concentrated force. The value of σ_{zz} first decreases and then oscillates for FSTM and EPM as r increases for both value of time.
Behaviour of shear stress component σ_{zr} w.r.t distance r due to concentrated force is shown in figure 4.19. The value of σ_{zr} increases for the range $0 \leq r \leq 2.2$ and then oscillates for FSTM as r increases for both values of time whereas for EPM, its value first decreases and then oscillates as r increases for time t=0.1 and t=0.5.

Fig. 20 shows the variation of pore pressure p w.r.t distance r due to concentrated force. The value of p decrease sharply for the range $0 \leq r \leq 2.1$ and then oscillates for FSTM as r increases for time t=0.1 whereas for the time t=0.5 the value of p shows initial decrease and then converges near the boundary surface.
Fig. 21 depicts the variation of temperature T w.r.t distance r for both FSTM and EPM due to concentrated force. The value of T increases sharply for the range $0 \leq r \leq 2.1$ and then starts oscillates for FSTM as r increases for time t=0.1 and t=0.5. In case of EPM, the value of T oscillates oppositely as r increases for both values of time. Behaviour of normal

stress component σ_{zz} w.r.t distance r due to force over circular region is shown in figure 4.22. The value of σ_{zz} first decreases and then oscillates for FSTM and EPM as r increases for both values of time.
Fig. 23 shows the variation of shear stress component σ_{zr} w.r.t distance r due to force over circular region. The value of σ_{zr} increases for the range $0 \leq r \leq 2.2$ and then oscillates for FSTM as r increases for both values of time whereas for EPM, its value first decreases and then oscillates as r increases for time t=0.1 and t=0.5.
Fig. 24 shows the variation of pore pressure p w.r.t distance r due to force over circular region. The value of p decreases sharply for the range $0 \leq r \leq 2.1$ and increases for the range $2.1 \leq r \leq 4$ for FSTM for time t=0.1 and for t=0.5 its value converges near the boundary surface.
Fig. 25 depicts the variation of temperature T w.r.t distance r due to force over circular region. The value of T increases sharply for the range $0 \leq r \leq 2.1$ and then starts oscillates for FSTM as r increases for time t=0.1 and t=0.5. In case of EPM, the value of T oscillates oppositely as r increases for both values of time.

FREQUENCY DOMAIN NORMAL FORCE

Behaviour of normal stress component σ_{zz} w.r.t distance r due to concentrated force is shown in figure 26. The value of σ_{zz} first increases monotonically and then start oscillating for FSTM as r increases for both value the time whereas for EPM its value first decreases and then oscillates as r increases for t=0.1 and t=0.5.
Fig. 27 shows the variation of shear stress component σ_{zr} w.r.t distance r due to concentrated force. The value of σ_{zr} first decreases for the range $0 \leq r \leq 2.4$ and then start oscillates for FSTM as r increases for both value the time where as its value oscillates oppositely as r increases for both value the time for EPM.
Fig. 28 shows the variation of pore pressure p w.r.t distance r due to concentrated force. The value of p converges near the boundary surface for the time t=0.1 whereas for t=0.5 its value first decreases for the range $0 \leq r \leq 2.5$ and then start oscillates for FSTM as r increases.
Fig. 29 depicts the variation of temperature T w.r.t distance r due to concentrated force. The value of T first decreases and then start oscillates for FSTM and EPM as r increases for both value the time

PRESSURE SOURCE

Fig. 30 shows the variation of normal stress component σ_{zz} w.r.t distance r due to concentrated force. The value of σ_{zz} first decreases sharply for the range $0 \leq r \leq 2.1$ and then start oscillates for the time t=0.1 where as for t=0.5 its value first increases and then start oscillates for FSTM as r increases.
Behaviour of shear stress component σ_{zr} w.r.t distance r due to concentrated force is shown in figure 31. The value of σ_{zr} for FSTM first decreases sharply for the range $0 \leq r \leq 2.1$ and then start oscillates for the time t=0.1 whereas for t=0.5 its value converges near the boundary surface as r increases.
Fig. 32 shows the variation of pore pressure p w.r.t distance r due to concentrated force. The value of p for FSTM decreases sharply for the range $0 \leq r \leq 6$ and then become linear as r increases for both value the time.
Fig. 4.33 depicts the variation of temperature T w.r.t distance r due to concentrated force. The value of T for FSTM first increases for the range $0 \leq r \leq 2.5$ and then start oscillates for the time t=0.1 and t=0.5.

THERMAL SOURCE

Fig. 34 shows the variation of normal stress component σ_{zz} w.r.t distance r due to concentrated force. The value of σ_{zz} oscillates oppositely for FSTM and EPM as r increases for t=0.1 and t=0.5.
Fig. 35 depicts the variation of shear stress component σ_{zr} w.r.t distance r due to concentrated force. The value of σ_{zr} first increases and then oscillates for FSTM for both value the time and in case of EPM its value first increases for the range $0 \leq r \leq 1.1$ and then start oscillates for the time t=0.1 whereas for t=0.5 its value first increases and then start oscillates as r increases.
Fig. 36 shows the variation of pore pressure p w.r.t distance r due to concentrated force. The value of p for FSTM decreases sharply for the range $0 \leq r \leq 4.5$ and then starts increasing for time t=0.1 whereas for t=0.5 its value converges near the boundary surface as r increases.
Fig. 37 shows the variation of temperature T w.r.t distance r due to concentrated force. The value of T converges near the boundary surface for FSTM for both value the time and in case of EPM its value oscillates oppositely for the time t=0.1 and t=0.5.

V. CONCLUSION

The work presented in this chapter provides a mathematical model to obtain the solutions of displacement, stress, pore pressure and temperature change due to various sources by using the Laplace and Hankel transforms. Various sources are taken to illustrate the application of the approach. Some particular cases of interest are also deduced.

In time domain, near the application of the source porosity effect increases the value of σ_{zz} and T for the normal force and for thermal source and away from the source due to porosity effect the value of σ_{zz} oscillates. Although there is difference in their magnitude values. Also porosity effect decreases the values of σ_{zr} for the force in normal direction but increase the values for pressure source.

In frequency domain, near the application of the source porosity effect decreases the value of σ_{zz} and T for the normal force and thermal source whereas the value of σ_{zr} increases for the force in normal direction and away from the source they have oscillatory behaviour in all the cases for both type of sources with difference in their magnitude values.

Near the application of the source the value of p decreases for the normal force and pressure source whereas it shows opposite behaviour for thermal source for both types of sources and away from the source it has oscillatory behaviour with difference in their magnitude values.
An appreciable porosity effect is observed on the components of stress, pore pressure and temperature change on the application of ring and disc loads. Near the application of the load, the porosity effect increases the value of σ_{zz} , p and decreases the value of σ_{zr} ,T and away from the source these values oscillates with the difference in their magnitude values.

REFERENCES

[1]. M.A. Biot , "General theory of three dimensional consolidation",J. Appl. Phys.12(2), 155-161(1941).
[2]. G.B.Liu ,et al.," Thermo-elastodynamic response of a spherical cavity in saturated poroelastic medium", Appl.Math.Model.34(8),2203-2222 (2010a).
[3]. G.B.Liu ,et al.," Mode of a spherical cavity's thermo-elastodynamic response in a saturated porous medium for non-torsional load", Comput. Geotech. 37(7), 381-390(2010b).
[4]. Y.Abousleiman and S. Ekbote ," Solutions for the inclined borehole in a porothermoelastic transversely isotropic medium", J. Appl. Mech. 72(2),102-114(2005).
[5]. R.Kumar and B.S. Hundal ," Symmetric wave propagation in a fluid saturated incompressible porous medium", J. Sound and Vibration 96(3),179-188(2004).
[6]. R. Kumar and Rupender,"Elastodynamics of axi-symmetric deformation in magneto-micropolar generalized thermoelastic medium",*Appl. Math. Mech. -Engl. Ed.* 30(1),39–48(2009) .
[7]. B.Bai and T.Li ," Solution for cylindrical cavety in saturated thermoporoelastic medium",Acta Mech. Solida Sinica 22(1),85-92(2009).
[8]. B.Bai , "Thermal response of saturated porous spherical body containing a cavity under several boundary conditions", Journal of thermal stresses 36(11), 1217-1232(2013).
[9]. M.Jabbari and H.Dehbani ," An exact solution for classic coupled thermoelasticity in axisymmetric cylinder", Journal of Solid Mechanics 2(2),129-143(2010).
[10]. M.Jabbari and H. Dehbani, "An exact solution for quasi-static poro- thermoelasticity in spherical coordinate", Iranian Journal of Mechanical Engineering 12(1), 86-108(2011).
[11]. M.Jabbari , et al, "Thermal buckling analysis of functionally graded thin circular plate made of saturated porous materials", Journal of thermal stresses 37, 202-220(2014).
[12]. A.Belotserkovets and J.H. Prevost " Thermoporoelastic response of a fluid saturated porous sphere:An analytical solution",Int. Journal of Eng. Sci. 49(12),1415-1423(2011).
[13]. P.F. Hou , M.Zhao and j.u.Jiann-Wen ,"Three dimensional green's function for transversely isotropic thermoporoelastic biomaterial",J.Appl. Geophysics 95,36-46(2013).
[14]. R.Gelet ,B. Loret and N. Khalili ," Borehole stability analysis in a thermoporoelastic duel-porosity medium",Int.J.of Rock Mech. and Mining Sci. 50 ,65-76(2012).
[15]. X.Y. Li ,W. Chain and H.Y. Wang ,"General steady state solution for transversely isotropic thermoporoelastic media in three dimension and its applications", Europian Journal of Mechanics-A/Solid 29(3),317-326(2010).
[16]. S. Mukhopadhyay and R. Kumar ," Analysis of phase-lag effects on wave propagation in a thick plate under axisymmetric temperature distribution", Acta Mech 210,331–344(2010).
[17]. Apostolakis G. and Dargus , G.F. (2013), " Mixed variation principal for dynamic response of thermoelastic and poroelastic continua", Int. J. of Solid and Structure , vol.50, No. 5, pp. 642-650.
Hou, P.F. , Zhao, M. and Jiann-Wen , J.U. (2013), " The three dimensional green's function for transversely isotropic thermoporoelastic biomaterial", J.Appl. Geophysics , vol. 95, pp. 36-46.
[18]. He, S.M., Liu, W. and Wang , J.(2015), "Dynamic simulation of landslide based on thermoporoelastic approach", Computers and Geosciences, vol. 75, pp. 24-32.
Nguyen, H.T., Wong , H., Fabbri , A., Georgin, J.F. and Prudhomme , E.(2015), "Analytical study of freezing behaviour of a cavity in thermoporoelastic medium", Computers and Geotechnics , vol. 67, pp. 33-45.
Wu, D., Yu , L., Wang , Y., Zhao, B. and Gao , Y. (2015), "A refined theory of axisymmetric thermoporoelastic circular cylinder",European J. Mech. A/Solid ,In Press , Accepted Manuscript .
[19]. M. Jabbari and H. Dehbani ," An exact solution for classic coupled thermoporo elasticity in cylinderical coordinate", Journal of Solid Mechanics 1(4), 343-357(2009).

[20]. R.Kumar and S.Deswal, "Axisymmetric problem in a generalized micropolar thermoelastic half space",Int. J. App. Mech. and Engg. ,12(2),413-429(2007).

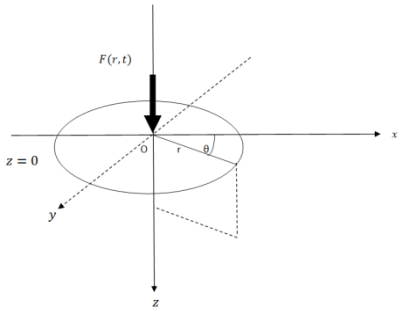

Fig. 1a Concentrated force or pressure source or thermal source $F(r,t)$ acting on the plane boundary $z=0$.

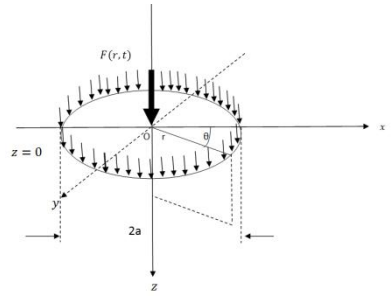

Fig. 1b. Force over the circular region or pressure source or thermal source $F(r,t)$, acting at the interface $z=0$.

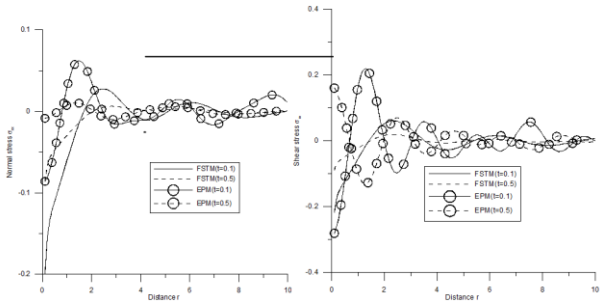

Fig .2 Variation of normal stress σ_{zz}w.r.t.distance r due to concentrated force in normal direction (time domain) Fig .3 Variation of shear stress σ_{zr}w.r.t.distance r due to concentrated force in normal direction (time domain)

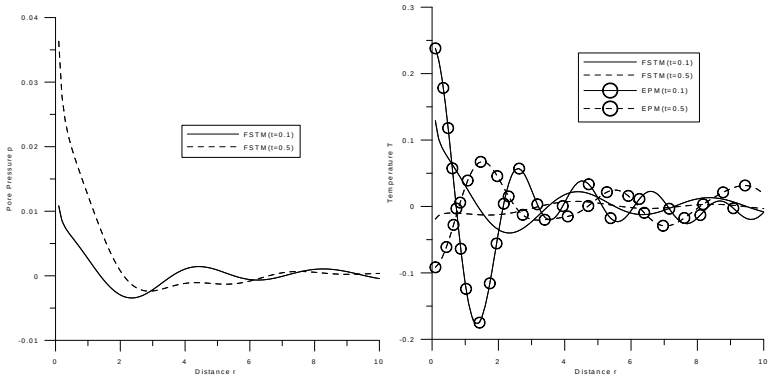

Fig .4 Variation of pore pressure p w.r.t.distance r due to concentrated force in normal direction (time domain) Fig.5 Variation of temperature T w.r.t.distance r due to concentrated force in normal direction (time domain)

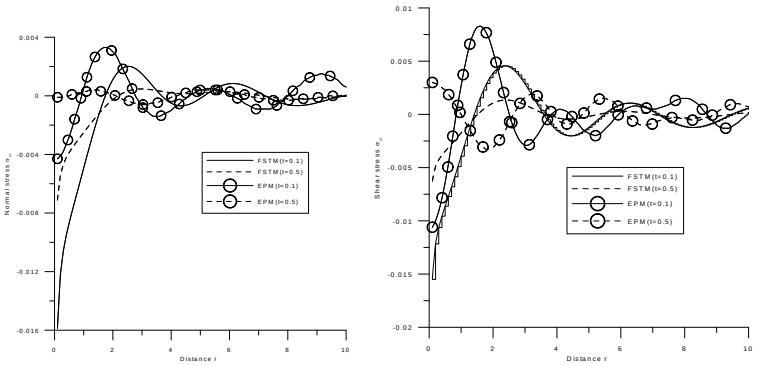

Fig .6 Variation of normal stress σ_{zz}w.r.t.distance r due to force over circular region in normal direction (time domain) Fig.7 Variation of shear stress σ_{zr}w.r.t.distance r due to force over circular region in normal direction (time domain)

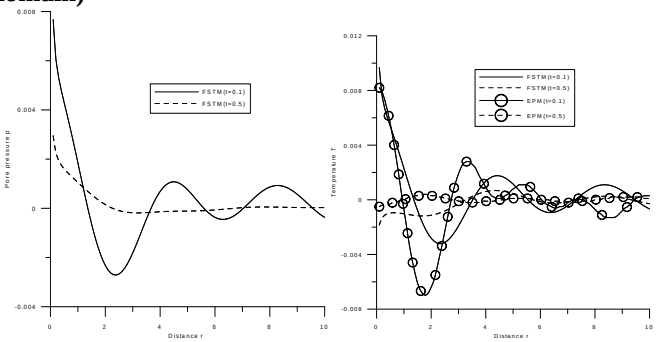

Fig.8 Variation of pore pressure p w.r.t.distance r due to force over circular region in normal direction (time domain) Fig.9 Variation of temperature T w.r.t.distance r due to force over circular region in normal direction (time domain)

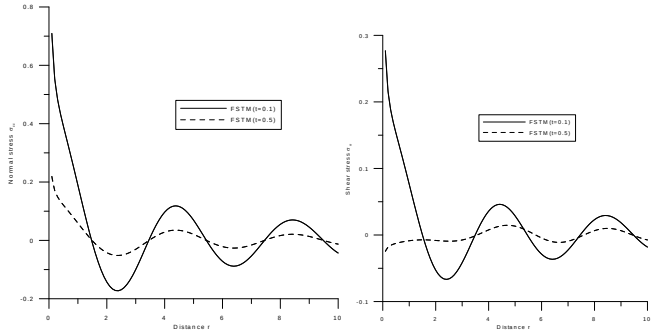

Fig.10 Variation of normal stress σ_{zz}w.r.t.distance r due to concentrated pressure source(time domain) Fig .11 Variation of shear stress σ_{zr}w.r.t.distance r due to concentrated pressure source(time domain)

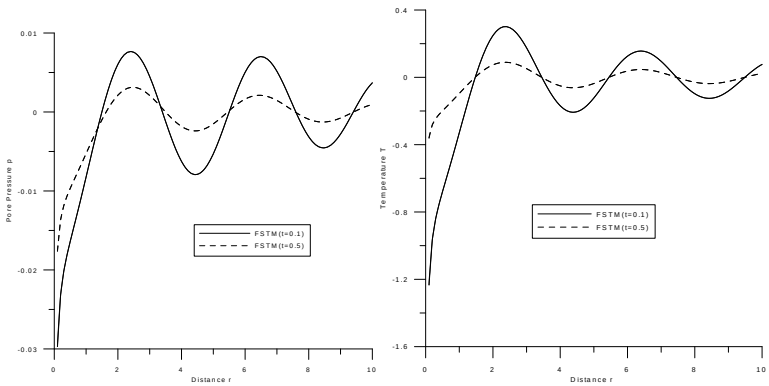

Fig.12 Variation of pore pressure p w.r.t.distance r due to concentrated pressure source (time domain) Fig.13 Variation of temperature T w.r.t.distance r due to concentrated pressure source(time domain)

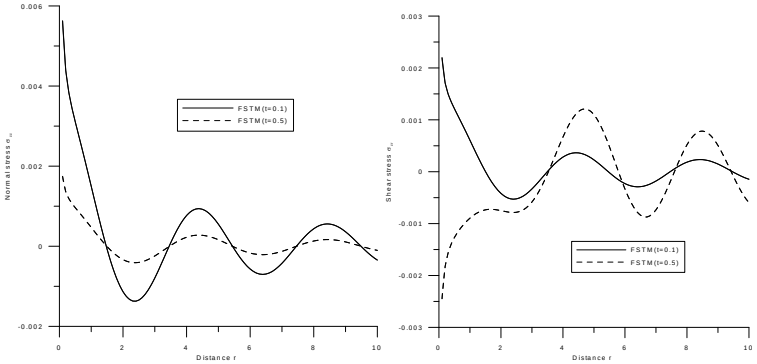

Fig .14 Variation of normal stress σ_{zz} w.r.t.distance r due to concentrated pressure source (time domain)
Fig 15 Variation of shear stress σ_{zr} w.r.t.distance r due to pressure source over circular region (time domain)

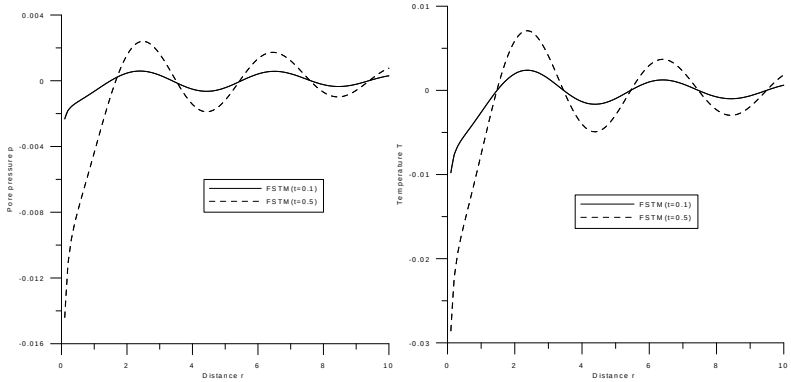

Fig 16 Variation of pore pressure p w.r.t.distance r due to pressure source over circular region (time domain) Fig 17 Variation of temperature T w.r.t.distance r due to pressure source over circular region (time domain)

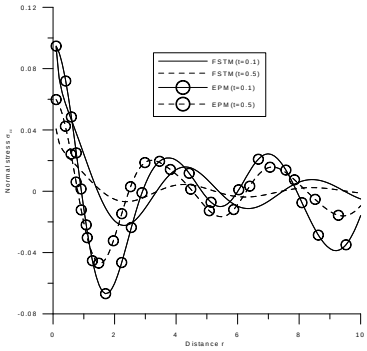

Fig .18 Variation of normal stress σ_{zz} w.r.t.distance r due to concentrated thermal source (time domain)

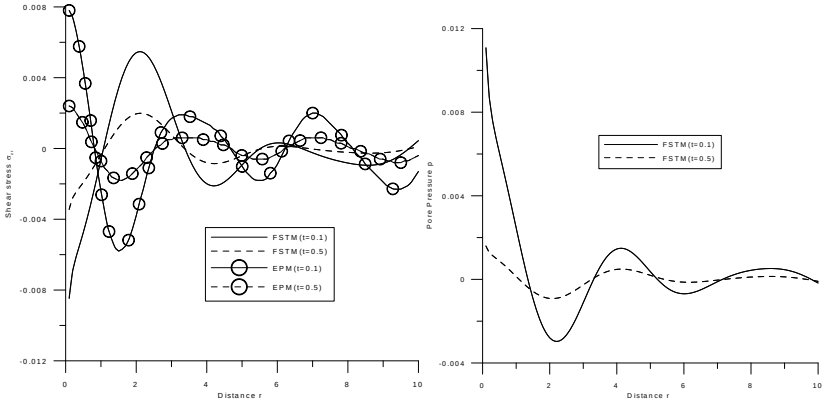

Fig .19 Variation of shear stress σ_{zr} w.r.t.distance r due to concentrated thermal source (time domain)Fig .20 Variation of pore pressure p w.r.t.distance r due to concentrated thermal source (time domain)

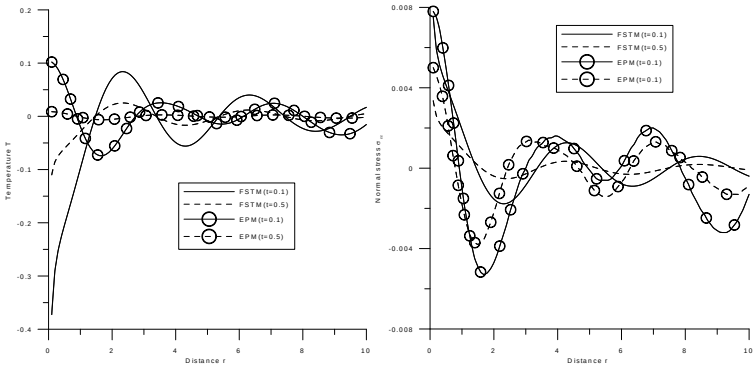

Fig 21 Variation of temperature T w.r.t.distance r due to concentrated thermal source (time domain) Fig .22 Variation of normal stressσ_{zz}w.r.t.distance r due to Thermal source over circular region (time domain)

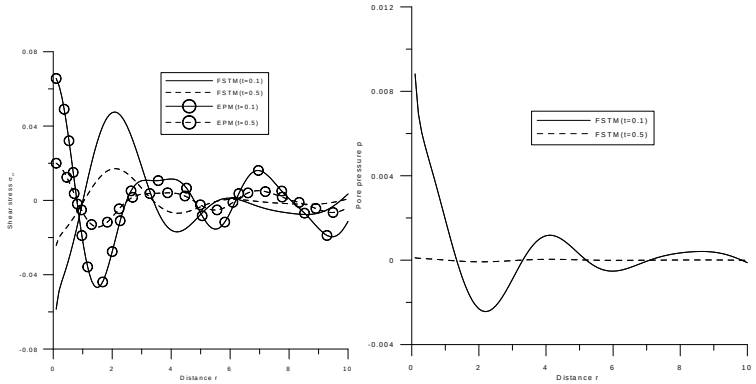

Fig.23 Variation of shear stressσ_{zr}w.r.t. distance r due to Thermal source over circular region (time domain) Fig 24 Variation of pore pressure p w.r.t.distance r due to Thermal source over circular region (time domain)

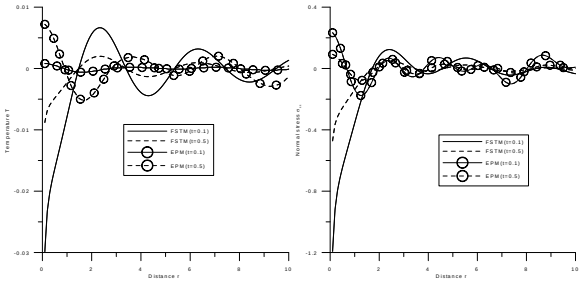

Fig .25 Variation of temperature T w.r.t.distance r due to Thermal source over circular region (time domain) Fig .26 Variation of normal stressσ_{zz}w.r.t.distance r due to concentrated force in normal direction (frequency domain)

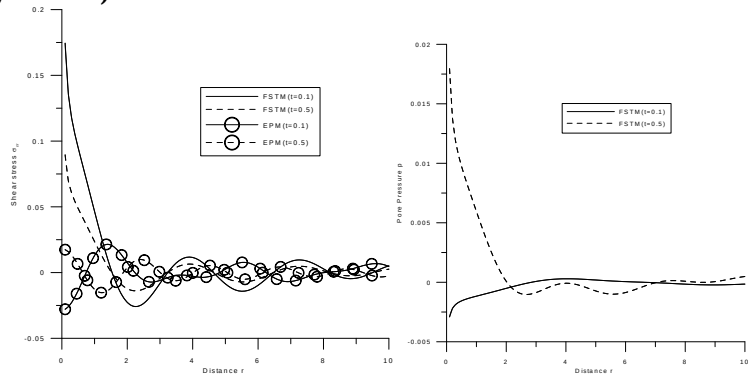

Fig .27 Variation of shear stress σ_{zr}w.r.t.distance r due to concentrated force in normal direction (frequency domain) Fig.28 Variation of pore pressure p w.r.t.distance r due to concentrated force in normal direction (frequency domain)

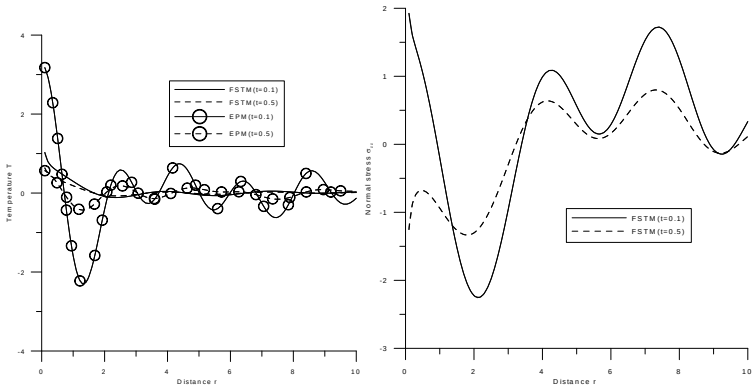

Fig .29 Variation of temperature T w.r.t.distance r due to concentrated force in normal direction (frequency domain) Fig .30 Variation of normal stress σ_{zz} w.r.t.distance r due to concentrated pressure source (frequency domain)

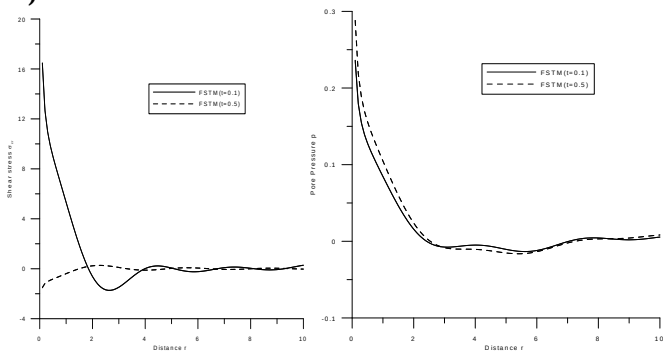

Fig .31 Variation of shear stress σ_{zr} w.r.t.distance r due to concentrated pressure source(frequency domain) Fig.32 Variation of pore pressure p w.r.t.distance r due to concentrated pressure source(frequency domain)

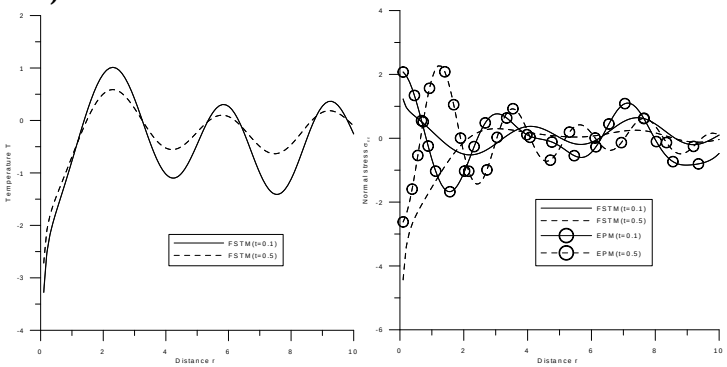

Fig .33 Variation of temperature T w.r.t.distance r due to concentrated pressure source(frequency domain) Fig .34 Variation of normal stress σ_{zz} w.r.t.distance r due to concentrated thermal source(frequency domain)

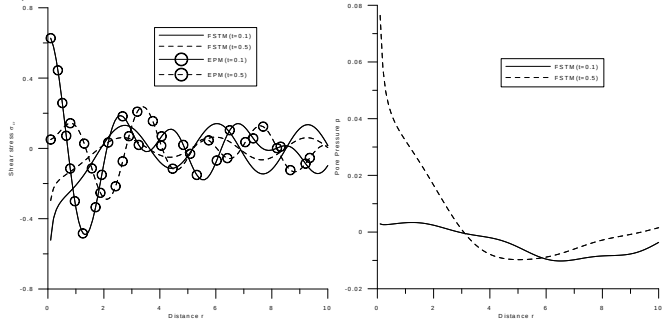

Fig .35 Variation of shear stress σ_{zr} w.r.t.distance r due to concentrated thermal source(frequency domain) Fig .36 Variation of pore pressure p w.r.t.distance r due to concentrated thermal source(frequency domain)

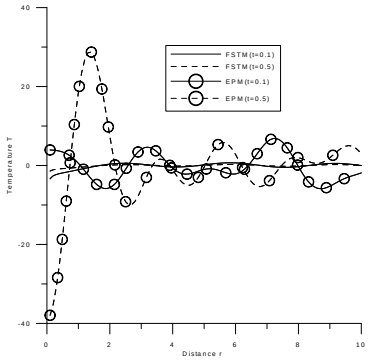

Fig .37 Variation of temperature T w.r.t.distance r due to concentrated thermal source(frequency domain)